

1 **Validation of Thorpe scale-derived vertical diffusivities against**
2 **microstructure measurements in the Kerguelen region**

3
4
5 Y.-H. Park^{1,*}, J.-H. Lee², I. Durand¹, C.-S. Hong²

6
7 ¹ MNHN-Sorbonne Universités (UPMC, Univ Paris 06)-CNRS-IRD, LOCEAN Laboratory,

8 Muséum National d'Histoire Naturelle, 43, rue Cuvier, F-75005 Paris, France

9 ² Korea Institut of Ocean Science & Technology, Ansan, Korea

10
11 *Corresponding author: yhpark@mnhn.fr

12 Tel: (+33) (0)1 4079 3170; Fax: (+33) (0)1 4079 5756

13

14

15

16

17

18

19

20

21

22

23

24

25

26

27 **Abstract**

28 The Thorpe scale is an energy containing vertical overturning scale of large eddies
29 associated with shear generated turbulence. This study investigates indirect estimates of vertical
30 diffusivities from the Thorpe scale method in the Polar Front region east of the Kerguelen
31 Islands based on fine scale density profiles gathered during the 2011 KEOPS2 cruise. These
32 diffusivities are validated in comparison with diffusivities estimated from the turbulence
33 dissipation rate directly measured via a TurboMAP microstructure profiler. The results are
34 sensitive to the choice of the diffusivity parameterization and the overturn ratio Ro , and the
35 optimal results have been obtained from the parameterization by Shih et al. (2005) and the $Ro =$
36 0.25 criterion, rather than the parameterization by Osborn (1980) and the $Ro = 0.2$ criterion
37 originally suggested by Gargett and Garner (2008).

38 The Thorpe scale-derived diffusivities in the KEOPS2 region show a high degree of spatial
39 variability, ranging from a canonical value of $O(10^{-5}) \text{ m}^2 \text{ s}^{-1}$ in the Winter Water layer and in the
40 area immediately north of the Polar Front to a high value of $O(10^{-4}) \text{ m}^2 \text{ s}^{-1}$ in the seasonal
41 thermocline between the surface mixed layer and the Winter Water. The latter high diffusivities
42 are found especially over the shallow plateau southeast of the Kerguelen Islands and along the
43 Polar Front that is attached to the escarpment northeast of the islands. The interaction of strong
44 frontal flow with prominent bottom topography likely causes the observed elevated mixing rates.

45

46 **1. Introduction**

47 Vertical mixing is a dominant factor in controlling vertical fluxes of heat, salt, and nutrients,
48 so the estimation of vertical (or diapycnal) diffusivities especially in the upper layer of the ocean
49 was one of the primary priorities of the physical component of the KEOPS2 cruise. During the
50 cruise, direct turbulence measurements were made at selected stations using a tethered quasi-
51 freefall profiler, TurboMAP, measuring the microstructure of velocity shear. An indirect method

52 for estimating vertical diffusivities using more accessible CTD (Conductivity-Temperature-
 53 Depth) density profiles is the Thorpe scale method (Thorpe, 1977). The objective of this study is
 54 to estimate the vertical diffusivities from fine scale density profiles using the Thorpe scale
 55 method and validate them in comparison with microstructure measurements collected via a
 56 TurboMAP during the KEOPS2 cruise.

57 The performance of the Thorpe scale method compared to microstructure estimates has been
 58 known to depend on the stratification of the water column and surface environment conditions
 59 affecting the ship motion. While good agreement between the two methods has been reported in
 60 low-latitude regions of high stratification and low winds (Ferron et al., 1998; Klymak et al.,
 61 2008), the application of the Thorpe scale method in the Southern Ocean could be compromised
 62 because of low stratification and extreme environments (Frants et al., 2013). The latter authors
 63 reported that the CTD-based fine structure methods overestimate microstructure diffusivities by
 64 one to two orders of magnitude in the southeastern Pacific and Drake Passage, claiming their real
 65 limitations in the Southern Ocean.

66 Another intriguing issue concerns the existence of two different parameterizations of vertical
 67 diffusivity K in terms of turbulence dissipation rate ε and buoyancy frequency N . Note that $N^2 =$
 68 $-(g/\rho_0)\rho_z$, where g is gravity, ρ_0 is a constant reference density, and ρ_z is a vertical gradient of
 69 potential density calculated at each depth over a vertical extent of 10 m.

70 For example, Osborn (1980) suggested a well-known parameterization as

71

$$72 \quad K = 0.2\varepsilon/N^2. \quad (1)$$

73

74 On the other hand, Shih et al. (2005) proposed a new parameterization for the energetic
 75 turbulence regime ($\varepsilon/\nu N^2 > 100$) based on the laboratory and numerical experiments as

76

$$K = 2\nu(\varepsilon/\nu N^2)^{1/2}, \quad (2)$$

77
78
79 where $\nu = (1.5 \text{ to } 1.8) \times 10^{-6} \text{ m}^2 \text{ s}^{-1}$ is the kinematic viscosity in the temperature range of 0 to 5°C
80 and $\varepsilon/\nu N^2$ is the turbulence intensity parameter. Note that for the moderate turbulence intensity
81 regime ($7 < \varepsilon/\nu N^2 < 100$), the parameterization of K by Shih et al. (2005) is same as (1) proposed
82 by Osborn (1980).

83 While the TurboMAP measurements lead to direct estimates of ε , the Thorpe scale method
84 gives its indirect estimates by making use of an empirical relationship between the Thorpe scale
85 and ε . These two (direct and indirect) estimates of ε can be applied to the above two
86 parameterizations of K , yielding a total of four kinds of K estimates (Osborn_ ε ,
87 Osborn_Thorpe, Shih_ ε , Shih_Thorpe) at each station of intercomparison. Because of their
88 utmost importance, the detailed procedures for the preliminary processing of CTD data as well as
89 for the detection and validation of overturns for calculating the Thorpe scale are given in section
90 2. These are largely based on a comprehensive paper by Gargett and Garner (2008), although we
91 have added some modifications. We will show in section 3 that the results are sensitive to the
92 choice of the K parameterization and to the criteria of the overturn validation. In section 4 we
93 present vertical diffusivities in the KEOPS2 area estimated from the optimally chosen
94 parameterization and overturn ratio. Discussion of a displacement shape method recently
95 proposed by van Haren and Gostiaux (2014) is given in section 5, followed by conclusions.

96

97 **2. Preliminary processing of CTD data**

98

99 CTD data used for deriving fine scale density profiles were collected during the October-
100 November 2011 KEOPS2 cruise aboard the R/V Marion Dufresne in the Polar Front (PF) region
101 east of the Kerguelen Islands (see Park et al., 2014, for details of the regional hydrography and
102 frontal circulation). Here we used a total of 22 CTD profiles gathered using two sets of Sea-Bird

103 SBE *9plus* sensors at stations shown in Fig. 1, where the concomitant TurboMAP stations are
104 shown circled. The CTD profiles mostly extend from the surface to the bottom, while the
105 TurboMAP measurements from the surface to about 400 m, limiting our validation of the Thorpe
106 scale method to the upper 400 m.

107 A critical step to a successful validation of the latter method resides in the minimization of
108 the effects of instrument noise and measurement errors, which may be due to the conductivity
109 cell's thermal lag, pressure reversals due to ship roll, and salinity spiking caused by the differing
110 time responses of the temperature and conductivity sensors (e.g. Gargett and Garner, 2008). A
111 series of procedures for processing CTD data are given below.

112 1) For minimizing thermal lag arising from the conductivity cell thermal mass effects, the
113 raw CTD data have been first processed using the Sea-Bird processing software
114 (http://www.seabird.com/pdf_documents/manuals/SBEDataProcessing_7.23.1.pdf). The data
115 processing module "Cell Thermal Mass" performs conductivity thermal mass correction, for
116 which we used typical values ($\alpha = 0.03$; $1/\beta = 7.0$) recommended for SBE *9plus* in the above
117 software.

118 2) Salinity spiking, which can be caused by misalignment of temperature and conductivity
119 with each other, was removed on acquisition from a pre-programmed SBE *9plus* deck unit by
120 advancing conductivity by 0.073 seconds. Therefore, there was no need to run the data
121 processing module "Align CTD".

122 3) Due to the effect of the ship heave motion on the hard-coupled CTD, the fall speed of
123 CTD continuously varies while scanning and can occasionally reverse sign for short periods. We
124 located segments of pressure reversals and edited out the data between successive encounters of
125 the same pressure, although such can be also done via the data processing module "Loop Edit".

126 4) At this stage, the CTD conductivity and salinity data were corrected with water bottle
127 salinity previously analyzed using a salinometer.

128 5) In order to further minimize any spike-like anomalies in property (salinity, potential
129 temperature, potential density) profiles, we applied a quadratic fit to successive 10-m segments
130 to detect and discard “extremely abnormal” anomalies surpassing 4 times the root mean square
131 (rms) anomaly relative to the fitting curve. About 0.03% of total scans are eliminated by this
132 process.

133 6) Our final CTD data processing consisted of averaging and subsampling profiles at regular
134 depth intervals. For this, we averaged the property profiles over a 10-cm window that is centered
135 at each depth incremented by a regular span of 10 cm. On average, about 2 to 3 scans enter into
136 this 10-cm averaging, which is roughly consistent with a mean fall rate of $\sim 0.9 \text{ m s}^{-1}$ of our 24
137 Hz CTD. This filters out any high-frequency random noise of a length scale less than 10 cm, thus
138 the smallest detectable overturn should be of 20 cm in vertical extent. Note also that most density
139 profiles start from 20 m below the sea surface because the near-surface measurements are often
140 found to be much contaminated probably by turbulence generated by the hull. These processed
141 density profiles form our basic data set used in the following section.

142

143 **3. Thorpe scale analysis**

144

145

146 ***3.1. Thorpe scale and vertical diffusivity***

147 A first step for detecting overturns generated by turbulence in a stratified water column
148 consists of sorting a potential density profile $\rho(z)$, which may contain inversions, into a stable
149 monotonic sequence without inversions. The vertical displacement necessary for generating the
150 stable profile is the Thorpe displacement d , and the Thorpe scale L_T is defined as the rms of d
151 within each overturn that is a region over which the sum of d drops back to zero (Dillon, 1982).

152 A classical measure of the overturning length is the Ozmidov scale L_O (Ozmidov, 1965)
153 defined as

154

155
$$\varepsilon = L_O^2 N^3. \quad (3)$$

156

157 Dillon (1982) suggested a linear relationship between L_T and L_O , such that

158

159
$$L_O = 0.8 (\pm 0.4) L_T, \quad (4)$$

160

161 although an exact linear relation between these two overturning scales cannot be expected due to
 162 spatial and temporal variability of the turbulent field (Ferron et al., 1998).

163 Inserting (3) and (4) into (1) and (2), the vertical diffusivity can be estimated indirectly

164 from L_T as

165

166
$$K = 0.128 L_T^2 N, \quad (5)$$

167

168 according to the Osborn parameterization, and as

169

170
$$K = 1.6 \nu^{1/2} L_T N^{1/2}, \quad (6)$$

171

172 according to the Shih parameterization. We give below a series of procedures necessary for an
 173 optimal estimation of L_T , thus of K from the Thorpe scale method.

174

175 ***3.2 Determination of a threshold noise level of density***

176 The major concern in the overturn validation is whether the identified overturns are false
 177 overturns associated with random noise and/or residual effects of salinity spiking. To prevent
 178 false overturns due to random noise, we followed an intermediate density profile method
 179 proposed by Gargett and Garner (2008) who modified a profile processing method of Ferron et

180 al. (1998). The Gargett and Garner method tracks only significant differences in the density
181 profile, where a significant difference is defined relative to a threshold noise level below which a
182 density difference is considered as due to random noise. For this purpose, we have calculated the
183 rms of detrended density anomalies over successive 10-m segments for selected “well-mixed”
184 layers within the cruise data set. This yielded a mean value of $1.75 \times 10^{-4} \text{ kg m}^{-3}$. We considered
185 a multiple of 4 of the latter value, $7 \times 10^{-4} \text{ kg m}^{-3}$, as our threshold noise level. Note that the latter
186 value is close to $5 \times 10^{-4} \text{ kg m}^{-3}$ of Gargett and Garner (2008) who applied instead a multiple of 5
187 to a slightly smaller mean rms density anomaly of $1.0 \times 10^{-4} \text{ kg m}^{-3}$ obtained in the Ross Sea
188 region using a SBE *9plus* CTD.

189

190 **3.3 Creation of an intermediate density profile**

191 Once the threshold value is determined as above, building an intermediate density profile
192 is straightforward as clearly explained in Gargett and Garner (2008). In short, an intermediate
193 profile is created first from the top to the bottom, maintaining a constant density until a density
194 change greater than the threshold value. A similar profile starting from the bottom to the top is
195 also created and a final intermediate profile used here is the average of the two individual
196 (downward and upward) profiles. An example of this procedure for determining an intermediate
197 density profile is shown in Fig. 2.

198

199 **3.4 Validation of overturns**

200 Gargett and Garner (2008) reviewed several previous methods of overturn validation and
201 proposed a practical method using an overturn ratio, $R_o = \min(L^+/L, L^-/L)$, where L is the total
202 vertical extent of an overturn and L^+ (L^-) is the cumulative extent occupied by positive (negative)
203 Thorpe displacements. These authors found the T - S tightness method suggested by Galbraith and
204 Kelly (1996) unsatisfactory and did not recommend any further rejection based on any measure

205 of T - S tightness. Gargett and Garner (2008) reasoned that a single perfect overturn sampled
 206 straight through the middle would contain equal lengths (extents) of positive and negative
 207 displacements (or $R_o = 0.5$), and suggested a critical R_o value of 0.2, below which the prospect
 208 overturn is suspected of being caused by residual salinity spiking.

209 We found that the $R_o = 0.2$ criterion is not sufficient in our case, but the use of $R_o = 0.25$
 210 at least is rather necessary to detect the false overturns associated with suspicious density spiking.
 211 An example is given in Fig. 3 for station A3-1, where we observe four clear density spikes as
 212 indicated by red arrows. The overturns associated with first two spikes near 200 and 225 m have
 213 R_o values between 0.2 and 0.25 (Fig. 3c), thus can be considered as false overturns according to
 214 the ($R_o =$) 0.25 criterion, whereas the 0.2 criterion might have validated them as true overturns.
 215 The third spike just above 300 m has a R_o value much smaller than 0.2, thus can be easily
 216 discriminated as a false overturn even by the more stringent 0.2 criterion. The fourth spike just
 217 below 300 m reveals a R_o value so close to 0.25 that the 0.25 criterion appears to be absolutely
 218 necessary for invalidating the prospect overturn. In summary, all four suspected overturns can be
 219 safely discriminated as false overturns by our new criterion $R_o = 0.25$, whereas the previously
 220 proposed $R_o = 0.2$ criterion by Gargett and Garner (2008) fails to detect these false overturns,
 221 except for the one associated with the third spike just above 300 m. We will show below that
 222 these four suspicious overturns really correspond to false overturns.

223

224 **3.5 Sensitivity of the vertical diffusivity to its parameterization**

225 With the Thorpe scales L_T obtained based on the $R_o = 0.25$ criterion, we have calculated
 226 vertical diffusivities from the Osborn parameterization (Eq. 5) and the Shih parameterization
 227 (Eq. 6), denoted hereafter as K_{O_T} and K_{S_T} , respectively. The regions where no overturns are
 228 detected do not necessarily mean no vertical mixing, as already remarked by Ferron et al. (1998),
 229 but our method cannot resolve tiny overturns smaller than 20 cm, as mentioned in section 2. In

230 this case the corresponding diffusivities are set to $1 \times 10^{-5} \text{ m}^2 \text{ s}^{-1}$, a value corresponding to the
231 minimum value ($1.024 \times 10^{-5} \text{ m}^2 \text{ s}^{-1}$) of the TurboMAP-derived diffusivities estimated using the
232 Shih parameterization. The resulting diffusivities have been averaged over regular vertical
233 intervals of 10 m. These Thorpe scale-derived diffusivities at station A3-1 are compared in Fig. 4
234 with those calculated according to (1) and (2) using the TurboMAP-derived ε , denoted hereafter
235 as K_{O_E} and K_{S_E} , respectively (Fig. 4c). We also show in the same figure K_{O_T} and K_{S_T}
236 estimated using the $R_o = 0.2$ criterion, always in comparison with K_{O_E} and K_{S_E} (Fig. 4b).
237 Several interesting features appear. First, the Thorpe scale-derived diffusivities for the case of R_o
238 $= 0.2$ are systematically overestimated compared to the TurboMAP-derived diffusivities by up to
239 one to two orders of magnitude in the layer below 80 m, while the converse is true above it in the
240 surface mixed layer. Second, such an overestimation or underestimation in the Thorpe scale-
241 derived diffusivities is much more pronounced by an order of magnitude with the Osborn
242 parameterization (K_{O_T}) compared to the Shih parameterization (K_{S_T}). Third, the TurboMAP-
243 derived diffusivities from both parameterizations (K_{O_E} and K_{S_E}) agree with each other within a
244 factor of 2, on average, except for the surface mixed layer where the difference reaches up to an
245 order of magnitude. As compared to K_{S_E} , there appears to be a tendency of great overestimation
246 (slight underestimation) of K_{O_E} in the surface mixed layer (deeper layer below 80 m). Finally,
247 we observe the efficiency of our new overturn validation criterion, $R_o = 0.25$ (see Fig. 4c), which
248 yields a much closer agreement with different estimates at the above-mentioned four suspicious
249 false overturns, while the $R_o = 0.2$ criterion (see Fig. 4b) still yields there abnormal
250 overestimation in the Thorpe scale-derived diffusivities (as compared to microstructure
251 diffusivities). This confirms our previous conviction that the four suspected overturns represent
252 really false overturns which escape from detection with $R_o = 0.2$ but can be safely detected with
253 $R_o = 0.25$. We have verified similar features in several other stations too, and we will use
254 hereafter uniquely the $R_o = 0.25$ criterion for the detection of false overturns.

255 In order to statistically evaluate the sensitivity of the vertical diffusivity to its
 256 parameterization, we have calculated for all intercomparison stations and depths the ratio of the
 257 Thorpe scale-derived diffusivities and the TurboMAP-derived diffusivities, separately using the
 258 Osborn parameterization (K_{O_T}/K_{O_E}) and the Shih parameterization (K_{S_T}/K_{S_E}) (Fig. 5). There is
 259 a clear tendency of overestimation by the Osborn parameterization especially in the layer deeper
 260 than 100 m by up to two orders of magnitude or more (Fig. 5a). Such is much less evident with
 261 the Shih parameterization which shows a comparatively much compact variability of ratio within
 262 an order of magnitude around unity (Fig. 5b). On the other hand, in the surface layer above 100
 263 m there is an increasing negative tendency toward the surface for both parameterizations, as
 264 already mentioned. This is probably due to a very low stratification of the surface mixed layer,
 265 which prevents detection of moderate overturns whose density differences are smaller than our
 266 threshold noise level of $7 \times 10^{-4} \text{ kg m}^{-3}$.

267 Assuming a log-normal distribution of diffusivity ratios R_{dif} , the mean and standard
 268 deviation (std) of $\log(R_{dif})$ have been used for representing the basic statistics of R_{dif} . With the
 269 Osborn parameterization (Fig. 5c), the Thorpe scale-derived diffusivities below 200 m
 270 overestimate (compared to the TurboMAP-derived diffusivities) by a mean R_{dif} of ~ 4 , with a (± 1
 271 std) variability range of (0.7, 20), on average. The overestimation gradually diminishes toward
 272 the surface and changes its sign near 80 m to show a near surface peak of underestimation, with a
 273 mean R_{dif} of ~ 0.2 (0.01, 5). In contrast to this, the Shih parameterization (Fig. 5d) yields a much
 274 more reasonable agreement, with a mean R_{dif} close to unity (0.3, 3) over most of the water
 275 column, except for the surface layer showing always a general but somewhat reduced tendency
 276 of underestimation by ~ 0.4 (0.1, 2). Consequently, we conclude that the use of the Shih
 277 parameterization, rather than the Osborn parameterization, is highly desirable in the estimation
 278 of vertical diffusivities for our study area, which is also worthy of testing its broad applicability
 279 in the other sectors of the Southern Ocean.

280

281 4. Thorpe scale-derived vertical diffusivities in the KEOPS2 area

282

283

284

285 For all KEOPS2 density profiles, we have estimated the Thorpe scale-derived vertical
286 diffusivities K by applying the overturn ratio criterion $R_o = 0.25$ and the Shih parameterization.
287 Figures 6a and 6b represent the spatial distribution of K in the upper 400 m along the
288 approximately north-south (N-S) and east-west (E-W) oriented transects, respectively (see Fig. 1
289 for the position of stations). The 50-m depth-averaged K values are given in Table 1. Care is
290 warranted to cite the values for the top 50-m depth range because of the above-mentioned
291 underestimation tendency; a multiplication by 2 to 3 is rather recommended. The K distribution
292 is highly heterogeneous in both the vertical and horizontal directions, varying from a low level of
293 $< 2 \times 10^{-5} \text{ m}^2 \text{ s}^{-1}$ (areas with no color shading) mostly in the Winter Water and the layer below to
294 a relatively high level of $> 10^{-4} \text{ m}^2 \text{ s}^{-1}$ (areas encircled by white lines) observed predominantly in
295 the upper 150 m. The area-averaged mixing rate in the subsurface layer (200-400 m) over the
296 entire KEOPS2 area is $4 \times 10^{-5} \text{ m}^2 \text{ s}^{-1}$, a value close to recent estimates from microstructure
297 measurements in a similar layer (250-500 m) north of the Kerguelen Plateau by Waterman et al.
298 (2013). It is also of the same order of magnitude as strain-derived diffusivities from Argo float
299 profiles in the same area (Whalen et al., 2012; Wu et al., 2011). For comparison, somewhat
300 contrasting results have been reported in the PF region of Drake Passage; elevated subsurface
301 diffusivities of $O(10^{-4}) \text{ m}^2 \text{ s}^{-1}$ have been estimated from Thorpe scales and CTD strain by
302 Thompson et al. (2007), whereas direct microstructure measurements of turbulence levels by St.
303 Laurent et al. (2012) have rather revealed a much weaker background level of $O(10^{-5}) \text{ m}^2 \text{ s}^{-1}$ (see
304 also Waterhouse et al., 2014), similar to the estimates in the Kerguelen region.

305 The spatial K distribution appears to have some correlation with the regional frontal
306 circulation carrying different water masses. For example, in the N-S transect (Fig. 6a) the areas
of elevated diffusivities are mostly confined in the seasonal thermocline (50-150 m) above the

307 Winter Water ($T_{\min} < 2^{\circ}\text{C}$) developed to the south of the PF, with the exception over the
308 continental slope east of the Kerguelen Islands (TNS-7 to TNS-9) where the mixing rate is low.
309 The strongest diffusivities are found over the shallow plateau (~ 600 m) southeast of the islands
310 (TNS-10 and A3-1) and close to the PF over the northern escarpment northeast of the islands
311 (TNS-3 to TNS-5). Our results are consistent with similar previous results showing enhanced
312 turbulent levels in the regions where deep reaching strong flow meets a rugged or abrupt bottom
313 topography (Wu et al., 2011; St Laurent et al., 2012; Whalen et al., 2012; Waterman et al., 2013;
314 Waterhouse et al., 2014). On the other hand, the Winter Water layer (150-250 m) generally
315 coincides with the layer of diffusivity minimum. Also, the mixing rate in warmer waters north of
316 the PF (TNS-1, TNS-2) is quite low throughout the upper 400 m, resting close to its background
317 level of $O(10^{-5}) \text{ m}^2 \text{ s}^{-1}$.

318 The diffusivity estimates at A3-1 are similar in vertical structure but smaller in magnitude
319 by a factor of 4 than those estimated at the same station during the 2005 KEOPS1 cruise (Park et
320 al., 2008). Several factors may explain this difference. First, in Park et al. (2008) the
321 discrimination of false from true overturns was based on the criterion that a minimum density
322 difference of 0.0015 kg m^{-3} (or three times the estimated noise level of 0.0005 kg m^{-3}) is
323 necessary to validate an overturn. As will be seen later in the discussion section, such a density
324 difference criterion is inefficient to discriminate the false overturns associated with density
325 spikes. Therefore, the latter criterion tends to overestimate the mixing rates as compared to the
326 overturn ratio criterion which is found to be agreeably efficient especially with $R_o = 0.25$ (see
327 Figs. 3, 4). Second, Park et al. (2008) used the Osborn parameterization which is found to yield
328 mean diffusivities significantly higher by a factor of 4 compared to the Shih parameterization
329 adapted in the present study (see Fig. 5).

330 On the E-W transect (Fig. 6b), the spatial distribution of K is quite complex compared to
331 the N-S section and there does not appear any simple pattern that can be easily connected to the

332 frontal circulation of water masses. Nevertheless, we remark a relatively strong mixing rate of
333 $O(10^{-4}) \text{ m}^2 \text{ s}^{-1}$ over much of the water column at E-4W that is located close to the northward
334 flowing PF along the escarpment east of the Kerguelen Islands, while the weakest rate of $O(10^{-5})$
335 $\text{m}^2 \text{ s}^{-1}$ is observed at TEW-7 where warmer polar frontal zone waters flow southward (Park et al.,
336 2014) along with the southward retroflecting PF (see also Fig. 1b). Other stations on the section
337 show a highly undulating vertical structure with a moderate mixing rate less than $5 \times 10^{-5} \text{ m}^2 \text{ s}^{-1}$,
338 in general.

339

340 **5. Discussion and Conclusions**

341 *5.1 Comparison with a displacement shape method*

342 Recently, van Haren and Gostiaux (2014) suggested a new method of discriminating
343 various overturns and intrusions via inspection of displacement (d) shapes in a d - z plane. They
344 showed that depending on the displacement slopes z/d , the true overturns can be categorized into
345 different types of vortex, such as most frequent half-turn Rankine vortices ($1/2 < z/d < 1$) and
346 rather rare full-turn Rankine vortices ($z/d \sim 1$) or solid-body rotations ($z/d = 1/2$). These authors
347 recommended to use temperature profiles rather than density profiles if salinity-compensating
348 intrusions are negligible, because the density profiles are much noisier thus cause an
349 overestimate of turbulence parameters. They mentioned also that more or less equivalent results
350 (within a factor of 1.5) may be obtained with the density data only by imposing a limit of
351 discarding density variations smaller than $1 \times 10^{-3} \text{ kg m}^{-3}$, twice the expected noise level.

352 In our case of the upper layer of the Antarctic zone the temperature is not an adequate
353 parameter for investigating overturns because of its unstable vertical distribution, with a gradual
354 temperature increase with depth from the Winter Water ($T_{\min} < 2^\circ\text{C}$) centered at about 200 m to
355 the Upper Circumpolar Deep Water ($T_{\max} \sim 2.3^\circ\text{C}$) centered at about 700 m (Park et al., 2014).
356 Then, we have tested the method using corrected density profiles after discarding density

357 variations (relative to sorted density profiles) smaller than the proposed limit of $1 \times 10^{-3} \text{ kg m}^{-3}$
358 by van Haren and Gostiaux, (2014).

359 An example of the test is given in Fig. 7 for station A3-1 already discussed in Figs. 3 and
360 4 and where there exist four clear density spikes (red arrows). van Haren and Gostiaux (2014)
361 previously remarked that discarding density variations $< 1 \times 10^{-3} \text{ kg m}^{-3}$ unfortunately limits the
362 use of investigating the shape of displacements. Consistent with this remark, discriminating
363 various types of overturns by inspection of displacement shapes does not appear very obvious
364 (Fig. 7b). Nevertheless, we observe that the most significant displacements appear mostly in the
365 vicinity of the above four density spikes, with a rather marked asymmetry between positive and
366 negative displacements. As before, the mixing rates have been estimated using the Shih
367 parameterization (Eq. 6) and the Thorpe scales L_T of identified overturns. The red line in Fig. 7c
368 illustrates the resultant diffusivities averaged over intervals of 10 m, in comparison with those
369 from our best approach of the Thorpe scale method (using intermediate density profiles and
370 applying the overturn ratio criterion $R_o = 0.25$ and the Shih parameterization: black line) and the
371 TurboMAP measurements (blue line). Note that the latter two lines are borrowed from Fig. 4c.
372 Compared to our best approach and the TurboMAP data, the displacement shape method yields
373 in many places comparable diffusivities within a factor of 2, but with a great exception in the
374 vicinity of the above four density spikes where we observe a significant overestimation (relative
375 to the TurboMAP data) by as much as an order of magnitude. This indicates that in great contrast
376 to our approach, the displacement shape method does not able to discriminate the false overturns
377 associated with apparent density spikes (caused probably by a mismatch between the
378 temperature and conductivity sensors), the major cause of most false overturns in the oceans
379 (e.g., Galbraith and Kelley, 1996; Gargett and Garner, 2008).

380

381 **5.2 Concluding remarks**

382 We have validated the Thorpe scale-derived vertical diffusivities in the PF region east of
383 the Kerguelen Islands using more direct estimates from the TurboMAP microprofiler
384 measurements at selected stations during the KEOPS2 cruise. We have emphasized the need of a
385 careful treatment of raw CTD data to obtain density profiles as fine as possible but with a
386 maximum removal of random noise and measurement errors. Here we have used density profiles
387 of 10 cm scales, which can yield fine resolution diffusivities at scales up to 10 m after a suitable
388 vertical averaging. This vertical resolution is far finer by an order of magnitude compared to
389 other indirect strain and shear methods that use a vertical integration scale of the order of 200 m
390 (e.g., Thompson et al., 2007; Frants et al., 2013). A compelling argument for obtaining such
391 finely resolved diffusivities from the Thorpe scale method may be that they should provide, as
392 compared to coarser estimates from the strain and shear methods, detailed local information
393 useful for precisely evaluating the vertical fluxes of nutrients and other biogeochemical materials
394 across the seasonal thermocline.

395 Our comparative results are found to be sensitive to the choice of the parameterization of
396 diffusivity and the overturn validation criteria. The use of the Shih parameterization (Eqs. 2 and
397 6) combined with our overturn ratio criterion of $R_o = 0.25$ has yielded significantly better results
398 by a factor of 5 compared to the results from the Osborn parameterization (Eqs. 1 and 5) and the
399 $R_o = 0.2$ criterion suggested by Gargett and Garner (2008). The latter criterion ($R_o = 0.2$) appears
400 to be insufficient (too low) to detect most false overturns associated with apparent density spikes,
401 thus overestimating diffusivities. Moreover, the Osborn parameterization is shown to be much
402 more sensitive to such an overestimation compared to the Shih parameterization. This study
403 demonstrates that the Thorpe scale method remains as a useful tool for investigating the fine
404 scale diffusivities in the Southern Ocean if one makes judicious use of the combined Shih
405 parameterization and $R_o = 0.25$ criterion. This is in stark contrast to Frants et al. (2013) who

406 claimed the real limitations of the CTD-based fine structure methods in Drake Passage and the
407 eastern Pacific sector of the Southern Ocean.

408 The Thorpe scale-derived vertical diffusivities in the KEOPS2 region vary from a
409 background level of $O(10^{-5}) \text{ m}^2 \text{ s}^{-1}$ in the Winter Water layer to a relatively high level of $O(10^{-4})$
410 $\text{m}^2 \text{ s}^{-1}$ in the seasonal thermocline which is a transitional boundary layer between the Winter
411 Water and the surface mixed layer. The latter high diffusivity feature is especially pronounced at
412 stations over the shallow plateau southeast of the Kerguelen Islands and in the cold side of the
413 PF running along the escarpment northeast of the islands. This is consistent with the general
414 belief that the interaction of strong flow with rough or abrupt bottom topography produces high
415 internal wave energy and intensified turbulence (e.g., Ferron et al., 1998; Klymak et al., 2008; St
416 Laurent et al., 2012; Waterman et al., 2013). On the other hand, at stations immediately north of
417 the PF where warmer surface waters are encountered, diffusivity values are particularly low.

418 **Acknowledgements**

420 This work was supported by the French Research program of INSU-CNRS LEFE–CYBER (Les
421 enveloppes fluides et l'environnement –Cycles biogéochimiques, environnement et ressources),
422 the French ANR (Agence Nationale de la Recherche, SIMI-6 program, ANR-10-BLAN-0614),
423 the French CNES (Centre National d'Etudes Spatiales) and the French Polar Institute IPEV
424 (Institut Polaire Paul–Emile Victor). We thank the captain and crew of the R/V *Marion Dufresne*
425 for their professional contributions to various field experiments during the 2011 KEOPS2 cruise.
426 We are also grateful to S. Blain, project manager, and B. Queguiner, chief scientist, for their
427 great effort for making the KEOPS2 cruise successful. We thank two anonymous reviewers for
428 constructive comments which have significantly improved the original manuscript. All co-
429 authors of the present paper have benefited by the STAR program, a French-Korean research
430 collaboration program, for their mutual exchanges in 2012 and 2013. JHL was partially

431 supported by the National Research Foundation of Korea Grant funded by the Korean
432 Government (NRF-2009-C1AAA001-0093065) to participate in the KEOPS2 cruise.

433

434 **References**

435 Dillon, T. M.: Vertical overturns: A comparison of Thorpe and Ozmidov length scales. *J.*
436 *Geophys. Res.*, 87, 9601-9613, 1982.

437 Ferron, B., H. Mercier, K. Speer, A. Gargett and K. Polzin: Mixing in the Romanche fracture
438 zone. *J. Phys. Oceanogr.*, 28, 1929-1945, 1998.

439 Frants, M., G. M. Damerell, S. T. Gille, K. J. Heywood, J. MacKinnon and J. Springtall: An
440 assessment of density-based fines-scale methods for estimating diapycnal diffusivity in the
441 Southern Ocean, *J. Atmos. Oceanic Technol.*, 30, 2647-2661, doi: 10.1175/jtech-d-12-
442 00241.1, 2013.

443 Galbraith, P. S. and D. E. Kelley: Identifying overturns in CTD profiles. *J. Atmos. Oceanic*
444 *Technol.*, 13, 688-702, 1996.

445 Gargett, A. and T. Garner: Determining Thorpe scales from ship-lowered CTD density profiles. *J.*
446 *Atmos. Oceanic Technol.*, 25, 1657-1670, doi:10.1175/2008JTECHO541.1, 2008.

447 Klymak, J. M., R. Pinkel and L. Rainville: Direct breaking of the internal tide near topography:
448 Kaena Ridge, Hawaii. *J. Phys. Oceanogr.*, 38, 380-399, doi:10.1175/2007JPO3728.1,
449 2008.

450 Osborn, T. R.: Estimates of the local rate of vertical diffusion from dissipation measurements. *J.*
451 *Phys. Oceanogr.*, 10, 83-89, 1980.

452 Ozmidov, R. V.: On the turbulent exchange in a stably stratified ocean. *Izv. Acad. Sci., USSR*
453 *Atmos. Oceanic Phys.*, 1, 853-860, 1965.

454 Park, Y.-H., J. L. Fuda, I. Durand and A. C. Naveira Garabato: Internal tides and vertical mixing
455 over the Kerguelen Plateau. *Deep-Sea Res. II*, 55, 582-593, 2008.

- 456 Park, Y.-H., I. Durand, E. Kestenare, G. Rougier, M. Zhou, F. d'Ovidio, C. Cotté and J.-H. Lee:
457 Polar Front around the Kerguelen Islands: An up-to-date determination and associated
458 circulation of surface/subsurface waters. *J. Geophys. Res. Ocean*, 119,
459 doi:10.1002/2014JC010061, 2014.
- 460 Shih, L. H., J. R. Koseff, G. N. Ivey and J. H. Ferziger: Parameterization of turbulent fluxes and
461 scales using homogeneous sheared stably stratified turbulence simulations. *J. Fluid Mech.*,
462 525, 193-214, 2005.
- 463 St. Laurent, L. C., A. C. Naveira Garabato, J. R. Ledwell, A. M. Thurnherr, J. M. Toole, and A. J.
464 Watson: Turbulence and diapycnal mixing in Drake Passage. *J. Phys. Oceanogr.*, 42,
465 2143–2152, doi:10.1175/JPO-D-12-027.1, 2012.
- 466 Thompson, A. F., S. T. Gille, J. A. MacKinnon, and J. Sprintall: Spatial and temporal patterns of
467 small-scale mixing in Drake Passage. *J. Phys. Oceanogr.*, 37, 572–592,
468 doi:10.1175/JPO3021.1, 2007.
- 469 Thorpe, S. A.: Turbulence and mixing in a Scottish Loch. *Philos. Trans. Roy. Soc. London*,
470 286A, 125-181, 1977.
- 471 van Haren, H. and L. Gostiaux: Characterizing turbulent overturns in CTD-data. *Dyn. Atmos.*
472 *Ocean*, 66, 58-76, 2014.
- 473 Waterhouse A. F., J. A. MacKinnon, J. D. Nash, M. H. Alford, E. Kunze, H. L. Simmons, K. L.
474 Polzin, L. C. St. Laurent, O. M. Sun, R. Pinkel, L. D. Talley, C. B. Whalen, T. N. Hussen,
475 G. S. Carter, I. Fer, S. Waterman, A. C. Naveira Garabato, T. B. Sanford, and C. M. Lee:
476 Global pattern of diapycnal mixing from measurements of the turbulent dissipation rate. *J.*
477 *Phys. Oceanogr.*, 44, 1854-1872, doi :10.1175/JPO-D-13-0104.1, 2014.
- 478 Waterman, S., A. C. Naveira Garabato, and K. L. Polzin: Internal waves and turbulence in the
479 Antarctic Circumpolar Current. *J. Phys. Oceanogr.*, 43, 259–282, doi:10.1175/JPO-D-11-
480 0194.1, 2013.

481 Whalen, C., L. D. Talley, and J. A. MacKinnon: Spatial and temporal variability of global ocean
482 mixing inferred from Argo profiles. *Geophys. Res. Lett.*, 39, L18612, doi:[10.1029/
483 2012GL053196](https://doi.org/10.1029/2012GL053196), 2012.

484 Wu, L. X., Z. Jing, S. Riser, and M. Visbeck: Seasonal and spatial variations of Southern Ocean
485 diapycnal mixing from Argo profiling floats, *Nat. Geosci.*, 4, 363–366,
486 doi:[10.1038/ngeo1156](https://doi.org/10.1038/ngeo1156), 2011.

487

488

489

490

491

492

493

494

495

496

497

498

499

500

501

502

503

504

505

506 Table 1. 50-m averaged vertical diffusivities (in $10^{-5} \text{ m}^2 \text{ s}^{-1}$) at KEOPS2 stations estimated from
 507 the Thorpe scale method using the Shih parameterization and the $R_o = 0.25$ criterion.

508

Station	depth range (m)							
	0-50	50-100	100-150	150-200	200-250	250-300	300-350	350-400
TNS-10	44	37	34	2	6	1	5	2
TNS-9	22	5	1	4	2	1	6	19
TNS-8	18	8	1	8	1	3	6	7
TNS-7	2	2	1	1	2	2	12	5
TNS-6	34	11	7	4	2	6	3	2
TNS-5	16	18	13	1	9	9	5	2
TNS-4	67	19	5	1	1	11	1	2
TNS-3	16	22	27	2	2	3	6	1
TNS-2	1	1	1	1	1	5	1	1
TNS-1	1	4	3	1	1	3	1	1
TEW-1	20	4	NaN	NaN	NaN	NaN	NaN	NaN
TEW-2	1	1	NaN	NaN	NaN	NaN	NaN	NaN
TEW-3	1	4	2	3	1	21	2	1
TEW-4	1	2	5	4	2	2	7	2
TEW-5	1	6	1	3	2	8	4	4
TEW-6	1	2	7	1	2	4	1	5
TEW-7	1	1	7	1	1	2	3	2
TEW-8	2	4	1	2	2	11	7	9
A3-1	13	18	13	2	1	1	2	5
E-2	4	1	3	6	1	2	6	2
E-4W	9	19	24	14	19	7	1	9
F-L	6	5	6	18	2	3	6	3

509

510

511

512

513

514

515

516

517

518

519

Figures captions

520
521
522 Fig. 1. (a) Map showing the KEOPS2 CTD stations (red dots) on or close to two N-S and E-W
523 transects superimposed on the detailed bathymetry. The concomitant TurboMAP microstructure
524 profiler stations are indicated by blue circles. Isobaths greater than 500 m are given every 500 m
525 and the seabed shallower than 200 m (100 m) is lightly (darkly) shaded. (b) These stations are
526 also superimposed on a representative satellite image of chlorophyll concentration (colors) and a
527 surface geostrophic velocity field (arrows) constructed from the combined data sets from
528 altimetry and trajectories of drifters launched during the cruise. The geographical position of the
529 Polar Front (PF) is indicated. This figure (b) has been adapted from Park et al. (2014).

530
531 Fig.2. Sample section of intermediate profiles generated from the top (red), from the bottom
532 (blue), and from the average of these two (thick black) of a measured density profile (thin black),
533 following the method of Gargett and Garner (2008). The threshold density noise (0.0007 kg m^{-3})
534 used is indicated.

535
536 Fig.3. Sample illustration showing the (a) intermediate density profile, (b) Thorpe scales, and (c)
537 overturn ratios calculated at A3-1. Four suspicious false overturns associated with abnormal
538 spikes clearly apparent in the density profile are indicated by red arrows. Two criteria of
539 overturn validation are shown by coloured vertical lines in (c): blue for $R_o = 0.2$ and red for $R_o =$
540 0.25 .

541
542 Fig.4. Different diffusivity profiles at A3-1 calculated with different pairs of parameterization
543 (Osborn or Shih) and observational method (Thorpe scale L_T or TurboMAP-derived ϵ) using the
544 two overturn validation criteria of (b) $R_o = 0.2$ and (c) $R_o = 0.25$. Note that the four abnormal

545 spikes seen in (a), which being the repetition of Fig. 3a, give rise to great overestimation in the
 546 Thorpe scale-derived diffusivities with $R_o = 0.2$, but such a feature disappears completely with
 547 $R_o = 0.25$.

548
 549 Fig.5. Ratio profiles of the Thorpe scale-derived diffusivities and the TurboMAP-derived
 550 diffusivities at all intercomparison stations based on (a) the Osborn parameterization and (b) the
 551 Shih parameterization. Here, the $R_o = 0.25$ criterion is commonly used. (c) and (d) are same as (a)
 552 and (b) but for the mean (black) and standard deviation (grey) of all stations.

553
 554 Fig.6. Thorpe scale-derived diffusivity sections (calculated using the Shih parameterization and
 555 the $R_o = 0.25$ criterion) of the upper 400 m on (a) the N-S transect and (b) the E-W transect (top
 556 panels; see Fig. 1 for locations of the transects and stations). Diffusivity K values, which range
 557 from $1 \times 10^{-5} \text{ m}^2 \text{ s}^{-1}$ to $7 \times 10^{-4} \text{ m}^2 \text{ s}^{-1}$, are shown in $\log(K)$. White and black lines correspond to
 558 $1 \times K = 10^{-4} \text{ m}^2 \text{ s}^{-1}$ and $K = 5 \times 10^{-5} \text{ m}^2 \text{ s}^{-1}$, respectively, while the regions without colour shading
 559 to $K < 2 \times 10^{-5} \text{ m}^2 \text{ s}^{-1}$. For easy of interpretation in combination with the 3-D frontal circulation
 560 of water masses (see also Fig. 1), corresponding temperature sections (middle panels) and seabed
 561 profiles drawn from in situ station depths measured during the KEOPS2 cruise (bottom panels)
 562 are also shown.

563
 564 Fig.7. (a) Potential density profile in the 150-400 m layer at A3-1, with four clear density spikes
 565 being indicated by red arrows. (b) Displacement points (red dots) computed from corrected
 566 density data after discarding density variations smaller than $1 \times 10^{-3} \text{ kg m}^{-3}$. Displacement slopes
 567 $z/d = 1$ (solid) and $z/d = 1/2$ (dashed) are superimposed. (c) Diffusivity profile estimated from the
 568 displacement shape method (red) in comparison with those from our best approach (black) and

569 TurboMAP data (blue), all using the Shih parameterization. See the text for more details. Red
570 arrows indicate the location of the density spikes seen in (a).

571

572

573

574

575

576

577

578

579

580

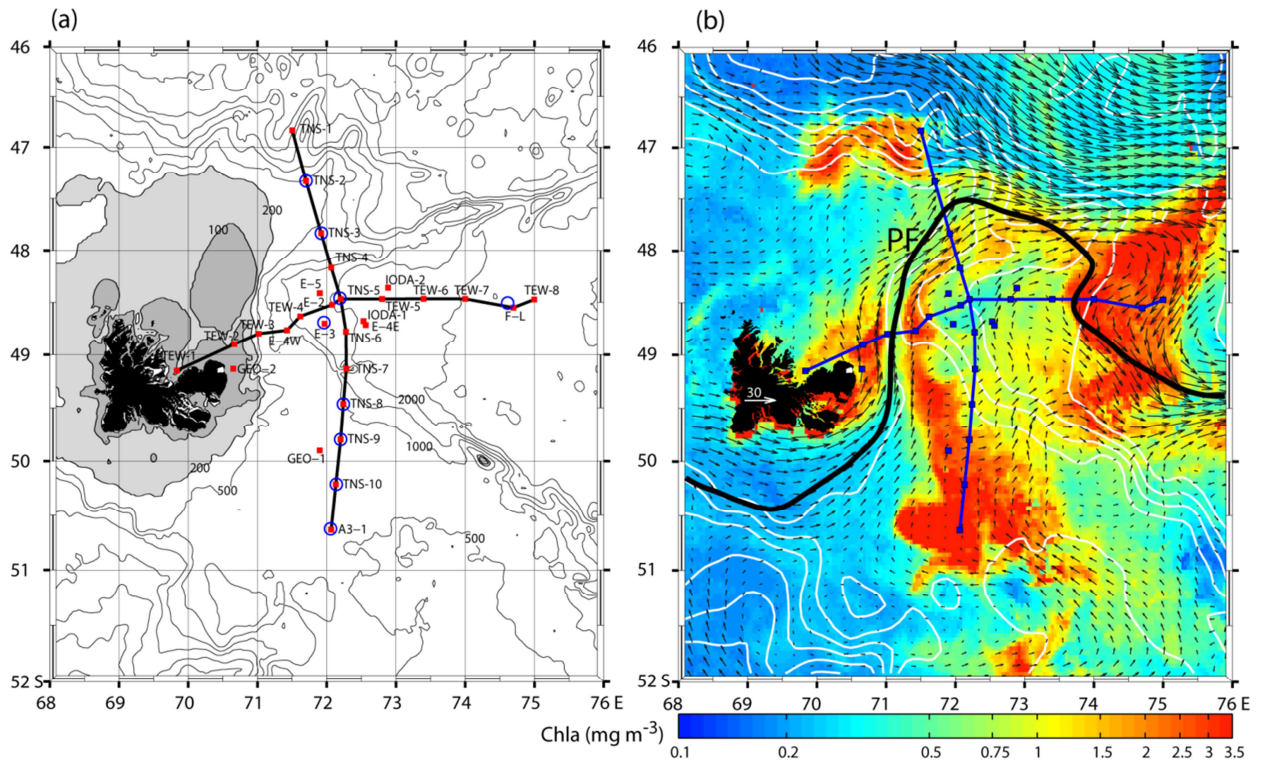
581

582

583

584

585



586

587

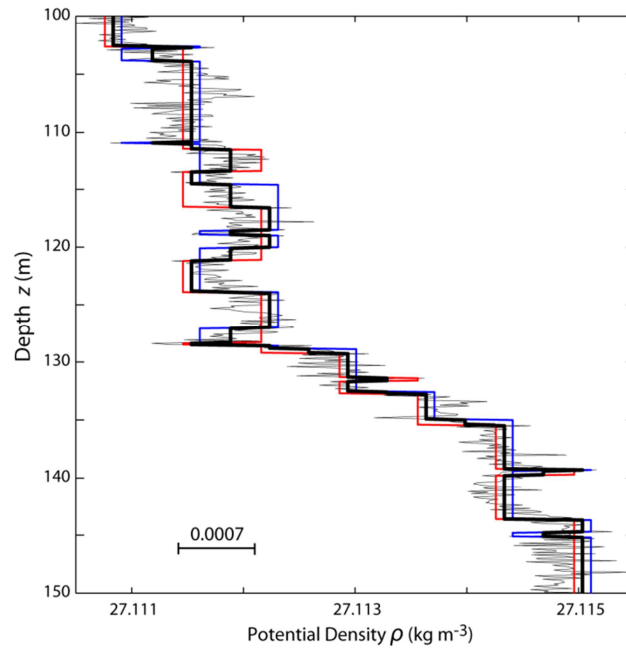
588 Fig. 1. (a) Map showing the KEOPS2 CTD stations (red dots) on or close to two N-S and E-W
 589 transects superimposed on the detailed bathymetry. The concomitant TurboMAP microstructure
 590 profiler stations are indicated by blue circles. Isobaths greater than 500 m are given every 500 m
 591 and the seabed shallower than 200 m (100 m) is lightly (darkly) shaded. (b) These stations are
 592 also superimposed on a representative satellite image of chlorophyll concentration (colors) and a
 593 surface geostrophic velocity field (arrows) constructed from the combined data sets from
 594 altimetry and trajectories of drifters launched during the cruise. The geographical position of the
 595 Polar Front (PF) is indicated. This figure (b) has been adapted from Park et al. (2014).

596

597

598

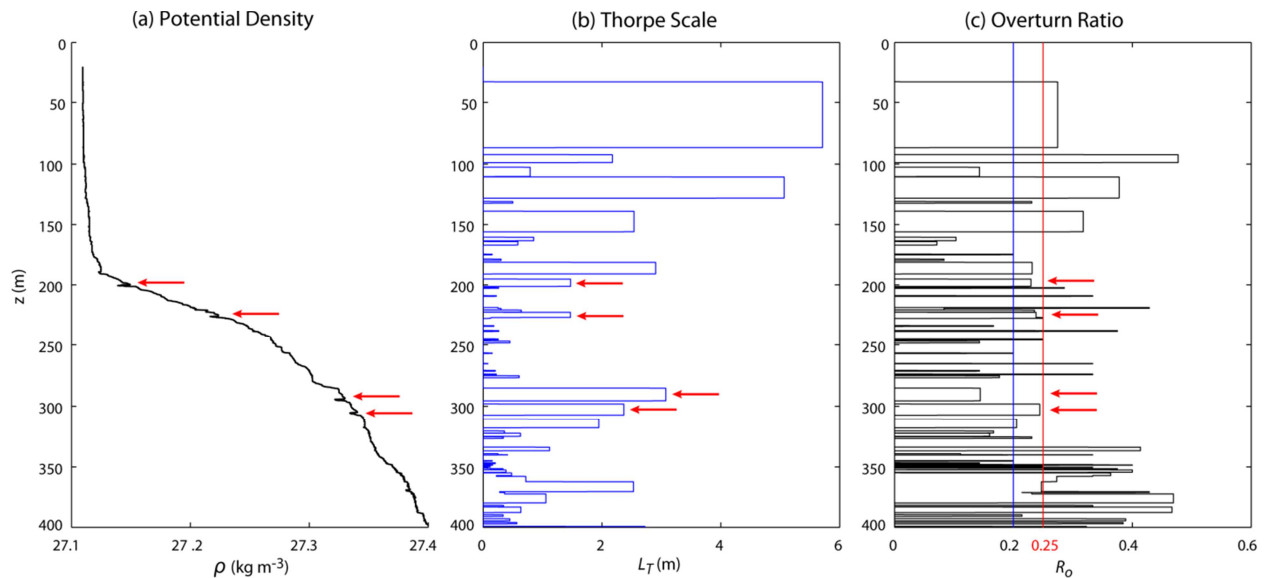
599



600

601

602 Fig.2. Sample section of intermediate profiles generated from the top (red), from the bottom
 603 (blue), and from the average of these two (thick black) of a measured density profile (thin black),
 604 following the method of Gargett and Garner (2008). The threshold density noise (0.0007 kg m^{-3})
 605 used is indicated.
 606

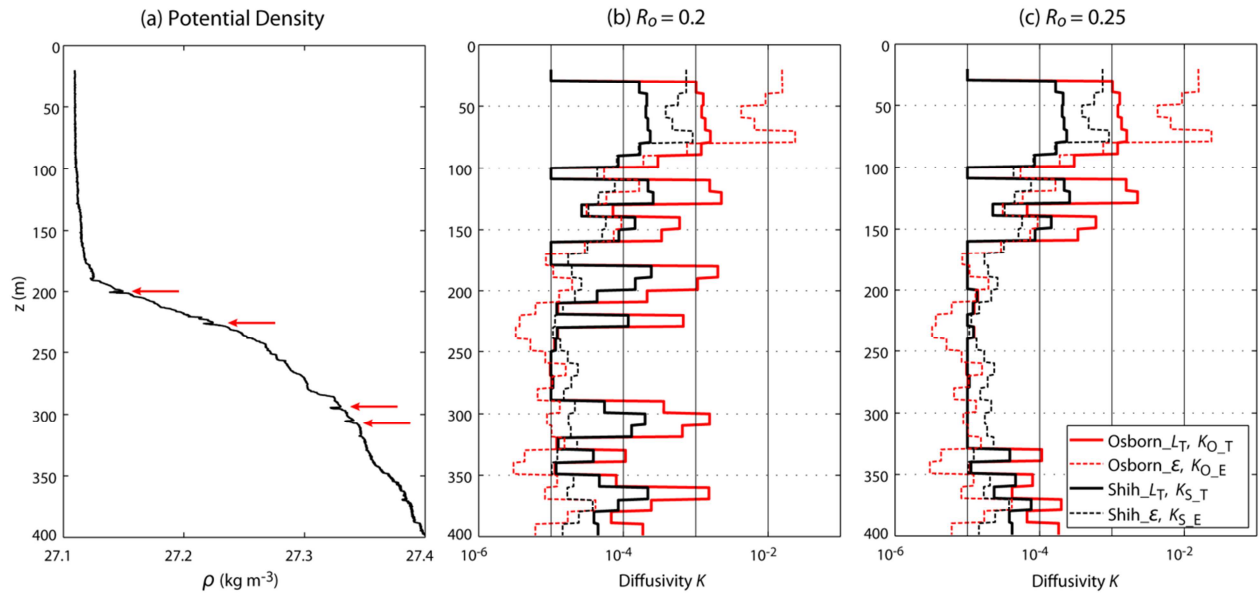


607

608

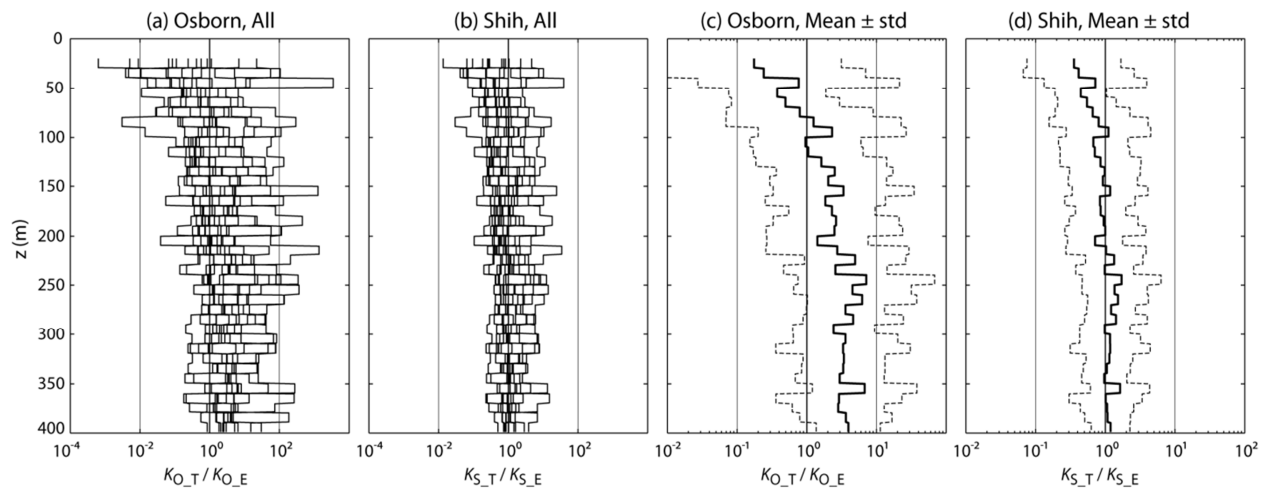
609

610 Fig.3. Sample illustration showing the (a) intermediate density profile, (b) Thorpe scales, and (c)
 611 overturn ratios calculated at A3-1. Four suspicious false overturns associated with abnormal
 612 spikes clearly apparent in the density profile are indicated by red arrows. Two criteria of
 613 overturn validation are shown by coloured vertical lines in (c): blue for $R_o = 0.2$ and red for $R_o =$
 614 0.25 .
 615



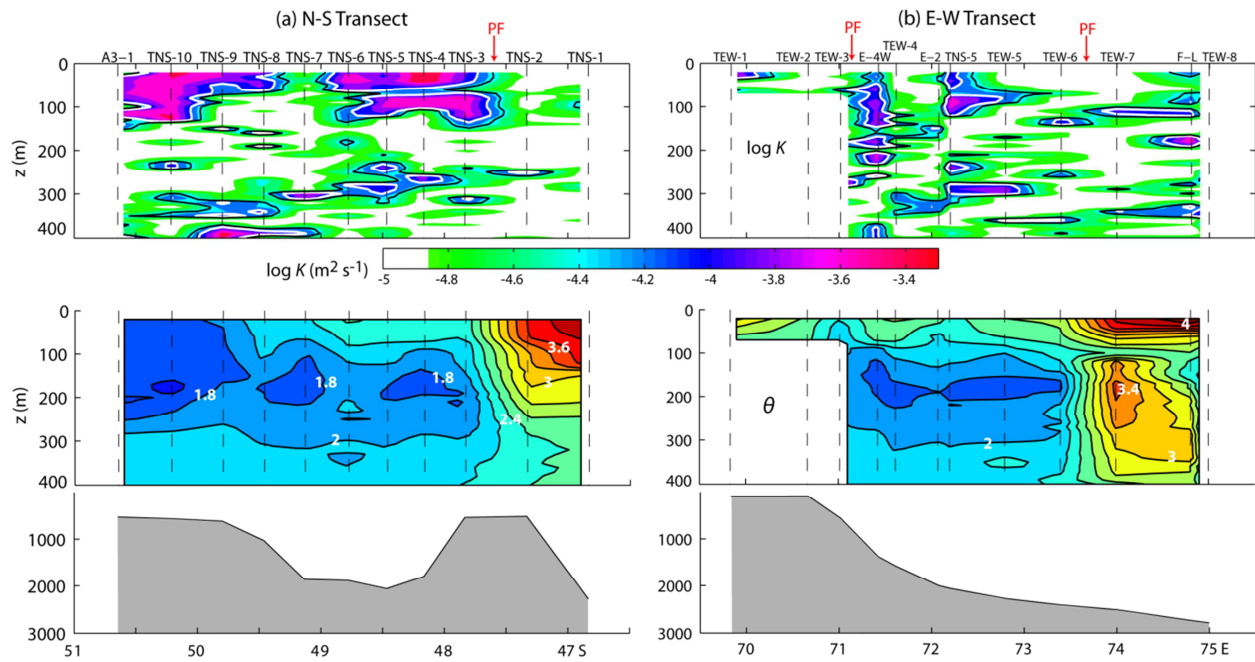
616
 617
 618 Fig.4. Different diffusivity profiles at A3-1 calculated with different pairs of parameterization
 619 (Osborn or Shih) and observational method (Thorpe scale L_T or TurboMAP-derived ε) using the
 620 two overturn validation criteria of (b) $R_o = 0.2$ and (c) $R_o = 0.25$. Note that the four abnormal
 621 spikes seen in (a), which being the repetition of Fig. 3a, give rise to great overestimation in the
 622 Thorpe scale-derived diffusivities with $R_o = 0.2$, but such a feature disappears completely with
 623 $R_o = 0.25$.

624
 625
 626
 627



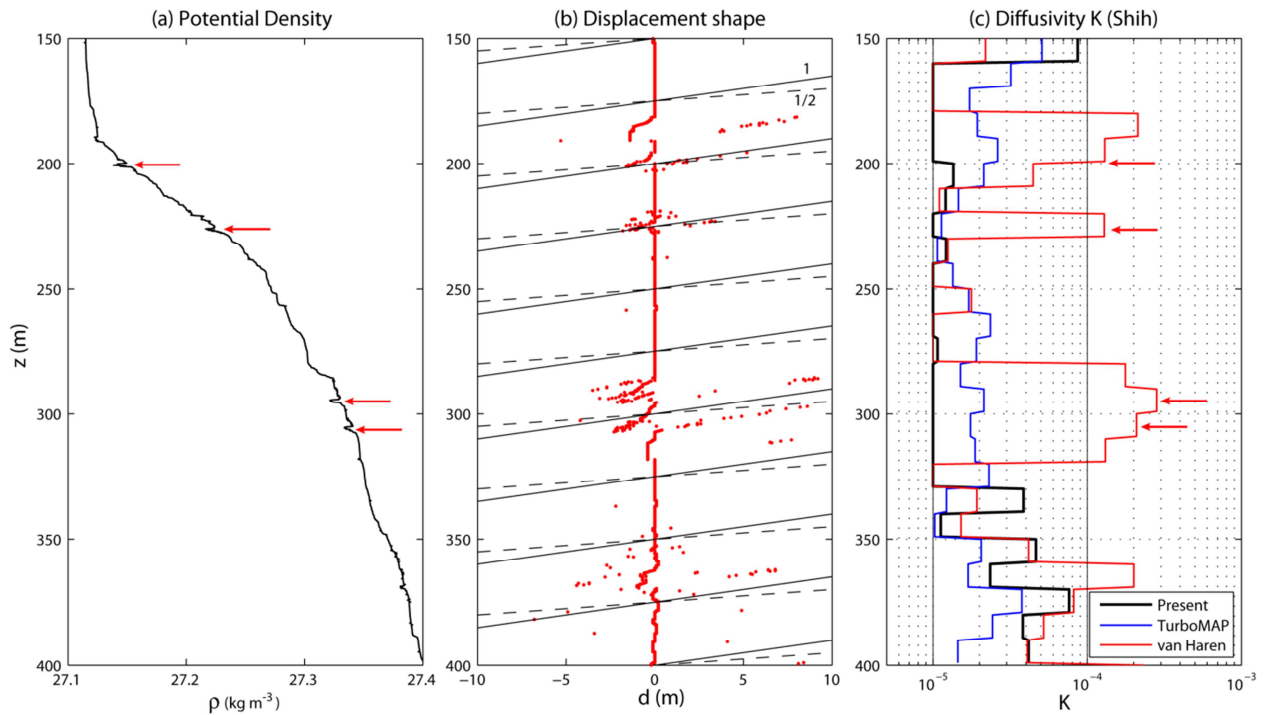
628
 629
 630
 631 Fig.5. Ratio profiles of the Thorpe scale-derived diffusivities and the TurboMAP-derived
 632 diffusivities at all intercomparison stations based on (a) the Osborn parameterization and (b) the
 633 Shih parameterization. Here, the $R_o = 0.25$ criterion is commonly used. (c) and (d) are same as (a)
 634 and (b) but for the mean (black) and standard deviation (grey) of all stations.

635
 636



637
 638
 639
 640
 641
 642
 643
 644
 645
 646
 647
 648
 649
 650
 651

Fig.6. Thorpe scale-derived diffusivity sections (calculated using the Shih parameterization and the $R_o = 0.25$ criterion) of the upper 400 m on (a) the N-S transect and (b) the E-W transect (top panels; see Fig. 1 for locations of the transects and stations). Diffusivity K values, which range from $1 \times 10^{-5} \text{ m}^2 \text{ s}^{-1}$ to $7 \times 10^{-4} \text{ m}^2 \text{ s}^{-1}$, are shown in $\log(K)$. White and black lines correspond to $K = 1 \times 10^{-4} \text{ m}^2 \text{ s}^{-1}$ and $K = 5 \times 10^{-5} \text{ m}^2 \text{ s}^{-1}$, respectively, while the regions without colour shading to $K < 2 \times 10^{-5} \text{ m}^2 \text{ s}^{-1}$. For easy of interpretation in combination with the 3-D frontal circulation of water masses (see also Fig. 1), corresponding temperature sections (middle panels) and seabed profiles drawn using in situ station depths measured during the KEOPS2 cruise (bottom panels) are also shown.



652
 653
 654
 655
 656
 657
 658
 659
 660
 661
 662
 663
 664
 665
 666
 667
 668
 669
 670
 671
 672
 673
 674

Fig.7. (a) Potential density profile in the 150-400 m layer at A3-1, with four clear density spikes being indicated by red arrows. (b) Displacement points (red dots) computed from corrected density data after discarding density variations smaller than $1 \times 10^{-3} \text{ kg m}^{-3}$. Displacement slopes $z/d = 1$ (solid) and $z/d = 1/2$ (dashed) are superimposed. (c) Diffusivity profile estimated from the displacement shape method (red) in comparison with those from our best approach (black) and TurboMAP data (blue), all using the Shih parameterization. See the text for more details. Red arrows indicate the location of the density spikes seen in (a).